,

Quantum Chemistry calculation of excited three centre systems: Theoretical study of $He^{2+} + H_2$ collisions.

L. F. Errea, A. Macías,* L. Méndez, B. Pons,† and A. Riera

Laboratorio Asociado al CIEMAT de Física Atómica y Molecular en Plasmas de Fusión.

Departamento de Química, Universidad Autónoma, 28049 Madrid, Spain

(Dated: March 14, 2003)

Abstract

Close-coupling calculations of single (dissociative and non dissociative) and double electron capture cross sections in $He^{2+} + H_2$ collisions in the range of impact energies 0.5 - 25 keV/amu are presented and compared with experimental data. The calculations have been carried out at the Franck-Condon level and employing both *ab initio* expansions, in terms of three-center electronic functions, and the independent particle model approximation. We discuss the mechanisms of the processes and the validity limits of these treatments.

*Instituto de Estructura de la Materia CSIC, Serrano 113 bis, 28006 Madrid, Spain

†Permanent address: Centre Lasers Intenses et Applications (UMR CNRS), Université de Bordeaux I, 351 Cours de Libération, 33405 Talence Cedex, France.

I. INTRODUCTION

The theoretical description of ion-H_2 collisions has been considered in several works of our group (see [1] and references therein) by using methods based on the application of the sudden approximation for the vibrational motion (see [2]). In a recent work [3] the fundamental process of electron capture in H^++H_2 has been studied, by applying a vibronic close-coupling treatment to discuss the limitations of the sudden vibrational approximation. One might think that similar calculations for He^{2+} +H_2 would only involve changing the ion charge in the program input, but the situation is completely different because of the presence of new physical processes. In fact, experimental data of ref. [4] show that, at low energies, besides non-dissociative single electron capture (NDSEC):

$$He^{2+} + H_2 \rightarrow He^+ + H_2^+ \ , \tag{1}$$

(analogous to electron capture in H^+-H_2), one has dissociative single electron capture (DSEC):

$$He^{2+} + H_2 \rightarrow He^+ + H + H^+ \ , \tag{2}$$

and two-electron capture (TEC):

$$He^{2+} + H_2 \rightarrow He + H^+ + H^+. \tag{3}$$

These reactions are unlikely in H^+-H_2. Moreover, for energies above 10keV/amu, ionizing processes (dissociative, non dissociative and transfer ionization) become competitive with charge transfer (see [5]).

Because of the complexity of this collisional process, there have been only a few theoretical treatments [6–8], and to our knowledge, ref. [8] is the first calculation in which reactions (1)-(3) are simultaneously taken into account. At first sight, the lack of reliable calculations for this particular collision is surprising, given that the HeH_2^+ system has only two electrons, which allows in principle for very precise *ab initio* molecular calculations. However, it must be noted that for the infinitely separated subsystems, the energy of the entrance channel lies above that of $He^+(1s)$ + H_2^{2+} + e^-, which is the limit of the two Rydberg series He(1snl) + H_2^{2+}, and $He^+(1s)$ + H_2^+(n λ). To solve the problem of performing calculations of such infinitely excited states, we have applied for other ion-H_2 systems [2, 9, 10], block-diagonalization techniques [11] , which are based on omitting some orbitals of

the quasimolecule from the set used to construct the Configuration Interaction (CI) basis. However, these techniques cannot be used in the present case, since states dissociating into $He^{2+} + H_2(1\sigma_g^2)$, $He^+(1s) + H_2^{2+}(n\lambda)$, and He(1snl) + H^+ + H^+ (to at least He(1s3l)) must be well represented if the calculations are to yield reliable values for the molecular data required to evaluate cross sections for reactions (1)- (3).

An important difference between He^{2+}-H_2 and other ion-H_2 collisions is the dominance of DSEC at low v, which takes place through transitions to dissociative electronic states of HeH_2^+, so that the use of expansions beyond the sudden approximation, [3], would require to include vibrational continuum states and limits our calculation to impact energies above 500eV/amu. Here, we have carried out the calculation by employing the Franck-Condon (FC) approximation. Another limitation appears at high energies, when ionization starts to be sizeable and large basis sets, including pseudostates, are required, which prevents employing an *ab initio* treatment. Instead, we have used at these high energies an effective potential formalism, called in this work independent particle model (IPM) (called independent electron approximation in ref. [12]), where one electron moves in an effective potential created by the nuclei and the other electron. More explicitly, we have used a time-independent model potential that allows us to employ large bases, in the present case formed by one-electron molecular orbitals (OEDM) ([13]), augmented by adding pseudostates [14] to describe the ionizing flux. Although IPM techniques are widely applied, the results are seldom compared to those from *ab initio* calculations in order to gauge their usefulness, in particular at low v [15]. In the present case, as we shall discuss in the next sections, the success of the IPM is a consequence of the fact that the mechanisms of reactions (1) and (2) are independent.

The interest of He^{2+}+H_2 collisions in fusion and astrophysical plasmas, has motivated a large number of experimental works [4, 5, 16–24], whose results are sometimes contradictory. Namely, the total cross section for reaction (1) of ref. [4] is, at $E \simeq 500$eV/amu, an order of magnitude smaller than the values recently reported by Juhász *et al.* [24] for the formation of He^+(2p) in the same reaction, and the data for total electron capture of [21] and [19] strongly disagree with previous experiments of [18]. These points are dealt with in a separate publication [8], where we included our best results (from *ab initio* or IPM methods) in each energy range. The aim of the present paper is to complement that work by discussing the mechanisms of the different processes and explaining the theoretical methods and computational procedures employed. The paper is organized as follows: In

section 2 we present the static part of our calculation: the evaluation of potential energy surfaces and dynamical couplings of the HeH_2^{2+} quasimolecule, which are then used to explain the collision mechanisms. In section 3 we summarize the theoretical methods used in the dynamical calculation. In section 4 we present and discuss our dynamical results. Our main conclusions are presented in section 5. Atomic units are used unless otherwise stated.

II. *AB INITIO* MOLECULAR CALCULATIONS

The potential energy surfaces and dynamical couplings of the HeH_2^{2+} quasimolecule depend on the internal coordinates R, ρ and θ, where R is the distance from the He nucleus to the midpoint of H-H internuclear axis, ρ is the H-H internuclear distance, and θ ($0 \leq \theta \leq 90^0$) is the angle between vectors $\boldsymbol{R}$ and $\boldsymbol{\rho}$. To calculate molecular energies and dynamical couplings, which include the corrections due to the CTF of [25], we have used the modified self-consistent-field multireference configuration interaction (SCF-MRCI) program MELD [26, 27]. The wavefunctions were obtained by performing CI calculations on the manifold spanned by all configurations that can be built from a set of SCF molecular orbitals of the $(He\text{-}H_2)^{2+}$ system obtained by using the set of contracted GTO's described below.

Preliminary calculations on the $(He\text{-}H_2)^{2+}$ system showed that the energy of the He^{2+} + H_2 entrance channel is much higher, for all R values, than those of the $He^+(1s)$ + $H_2^+(1\sigma_g)$ ones, while it interacts strongly, at R $\simeq$ 3 a_0. with channels correlated to $He^+(1s)$ + $H_2^+(2\sigma_g, 2\sigma_u)$, which involve dissociative states of the H_2^+ molecule. Since energy differences between electronic states of H_2^+ are much smaller than those between electronic states of the He^+ or He, and to have a good description of a number of the lower channels correlating to $He^+(1s)$ + H_2^{+*} (electronically excited) states, we have selected a basis set centered on each H atom that reproduces the energies of the first two electronic states of the H_2 molecule with good precision [28], and the first 8 MO's of the H_2^+ ion as compared to the exact OEDM values [13]. The basis set (given in tables I) is made up of 6 s and 5p primitive GTOs contracted to 4s and 3p respectively, plus two uncontracted (one s and one p) GTOs.

Regarding the basis set centered on the He nucleus (table II), and since there has been some discussion on whether the most important double capture states involve the He(1s3l) manifold, we have chosen one that is able to reproduce well up to He(1s4s,4p,4d) states; then, this set is made up from 12s, 8p and 5d primitive GTOs contracted to 5s, 5p and 3d

exponents	1s	2s	3s	4s	5s
33.865	0.00606	0.004330	-0.002290	0.002170	–
5.095	0.04155	0.03214	-0.1659	0.01631	–
1.159	0.2146	0.17515	-0.1039	0.09797	–
0.3255	0.3153	0.72985	-0.2944	0.5287	–
0.1027	0.02707	0.79651	0.3644	0.2394	–
0.0327	0.001500	0.66325	0.2976	-0.7978	–
1.0	–	–	–	–	1.0

exponents	1p	2p	3p	4p
0.75	0.09424	-0.05005	0.06492	–
0.5	-0.03347	0.07273	-0.2614	–
0.2	0.35483	-0.5004	0.2779	–
0.05	0.2147	-2.4265	-0.1158	–
0.02	-0.03817	-0.6222	-0.4226	–
1.0	–	–	–	1.0

TABLE I: Exponents and contraction coefficients of the GTOs centered on the hydrogen nuclei.

contracted GTOs.

In table III we present a list of (some) asymptotic energies at $R \to \infty$ and $\rho = 1.4$ a$_0$., corresponding to the two Rydberg series having a common ionization limit, plus the entrance channel and the states of interest whose energies are above that limit. Exact values for He states are obtained from Moore tables [29], from [28] for H_2 and from OEDM calculations for H_2^+. Differences between the two sets of energies listed in table III are of the order of a few mHartree for the states of interest (the He($1s^2$) + H_2^{2+} state plays no role in the charge transfer processes).

The energies of some adiabatic molecular states are shown in figure 1a as functions of R, for ρ=1.4 a$_0$ and θ=45^0. In our calculation the entrance channel is represented, at large R values ($R \simeq 10$ a.u.), by the root no. 28, and the $He^+(2l)$ + $H_2^+(1\sigma_g)$ channels by roots

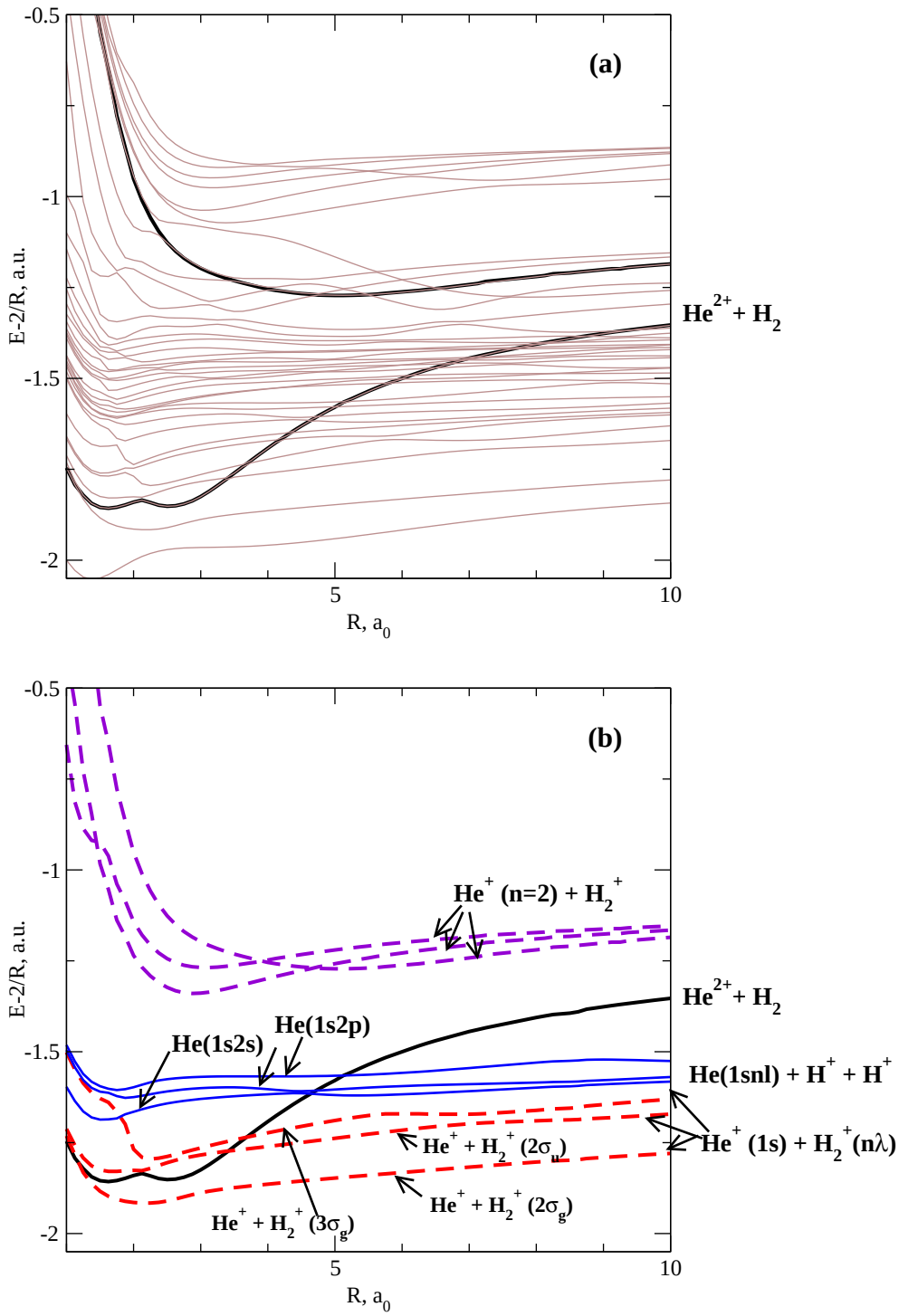

FIG. 1: Energies of the electronic states of the He H_2^{2+} quasimolecule for $\rho = 1.4a_0$ and $\theta = 45^0$. (a) Adiabatic energies of the states no 4-40, (b) Energies of the "diabatic states". The energies of the diabatic entrance channel and the lowest diabatic state correlating to $He^+(2l) + H_2^+(1\sigma_g)$ are also shown in (a) over-imposed to the adiabatic energies.

exponents	1s	2s	3s	
175.0	0.00412	0.00265	0.00234	
38.0	0.01484	0.00956	0.00855	
10.75	0.08722	0.05847	0.052555	
2.55	0.35091	0.27013	0.24942	
0.7875	0.50308	0.57451	0.57426	
0.305	0.18182	0.20438	0.22950	
exponents	4s	5s	6s	7s
0.125	1.2961	0.5296	0.6427	0.5485
0.0625	-0.5819	0.4453	0.6862	0.7208
0.075	0.44855	0.06791	-1.09191	-2.27534
0.0125	-0.4072	-0.02356	-0.5177	0.03115
0.0075	0.2491	0.01284	0.1108	1.65362
0.003125	-0.5076	-0.00243	-0.01636	-0.01793

exp.	1p	2p	3p	4p	exp.	1d	2d	3d
0.9	0.14248	–	-0.14556	–	0.0875	0.64882	–	-0.60237
0.27	0.48316	–	0.68081	–	0.0.025	0.51316	–	0.35806
0.09	0.50597	–	0.10465	–	0.0075	-0.05275	–	0.80062
0.025	0.01221	–	-1.83797	–	0.0025	–	0.02242	–
0.007	–	1.43544	–	1.46937	0.00077	–	-0.00693	–
0.0025	–	-0.82025	–	-0.92357	–	–	–	–
0.0005	–	0.21065	–	0.22321	–	–	–	–
0.0001	–	-0.06019	–	-0.060031	–	–	–	–

TABLE II: GTOs centered on the He nucleus

nos. 32-34. All avoided crossings between the energy of the entrance channel and the lower lying states, correlated to DSEC or TEC channels, are extremely narrow down to values of $R \simeq 3.0a_0$, indicating that, except at very low impact energies, all these avoided crossings are traversed diabatically. This point is confirmed by the extremely sharp radial couplings

State		E (Exact)	E (calc)
He^+(n=2) + $H_2^+(1\sigma_g)$		-1.0700	-1.0670
He^{2+} + $H_2(1\sigma_g^2)$		-1.1744	-1.1714
- - - He^+(1s)+ H_2^{2+} + e^-		-1.2857	-1.2847
-	-		
-	-		
-	-		
-	He(1s4p)+ H_2^{2+}	-1.3169	-1.3140
-	He(1s4d)+ H_2^{2+}	-1.3170	-1.3142
-	He(1s4s)+ H_2^{2+}	-1.3193	-1.3178
-	He(1s3p)+ H_2^{2+}	-1.3408	-1.3380
-	He(1s3d)+ H_2^{2+}	-1.3413	-1.3402
-	He(1s3s)+ H_2^{2+}	-1.3470	-1.3457
-	He(1s2p$_z$) + H_2^{2+}	-1.4095	-1.4055
-	He(1s2p$_x$) + H_2^{2+}	-1.4095	-1.4055
-	He(1s2s)+ H_2^{2+}	-1.4316	-1.4295
-			
-			
-			
He^+(1s)+ $H_2^+(3\sigma_g)$		-1.5131	-1.5105
He^+(1s)+ $H_2^+(2\sigma_u)$		-1.5344	-1.5341
He^+(1s)+ $H_2^+(2\sigma_g)$		-1.6806	-1.6796
He^+(1s)+ $H_2^+(1\pi_u)$		-1.7397	-1.7395
He^+(1s)+ $H_2^+(1\sigma_u)$		-1.8978	-1.8974
	He(1s^2)+ H_2^{2+}	-2.1890	-2.1670
He^+(1s)+ $H_2^+(1\sigma_g)$		-2.5700	-2.5694

TABLE III: Energies in Hartree for $\rho = 1.4a_0$ and in the limit $R \to \infty$

between the corresponding states, and we have checked this by carrying out Landau-Zener estimates of the transition probabilities at these avoided crossings. From fig. 1a it is apparent that the treatment of processes (1)-(3) cannot be carried out with the adiabatic correlation diagram including over 30 states, so that, we have built up a "diabatic" entrance channel by traversing diabatically the above mentioned narrow avoided crossings. For example at one avoided crossings between the energies of the adiabatic states ϕ_k, ϕ_{k+1}, we define a diabatic set ϕ_k^d, ϕ_{k+1}^d in the usual form [30]:

$$\begin{aligned} \phi_k^d &= \cos\alpha\phi_k + \sin\alpha\phi_{k+1} \\ \phi_{k+1}^d &= -\sin\alpha\phi_k + \cos\alpha\phi_{k+1} \end{aligned} \tag{4}$$

with

$$\left\langle \phi_k \left| \frac{\partial}{\partial R} \right| \phi_{k+1} \right\rangle = -\frac{\mathrm{d}\alpha}{\mathrm{d}R} \tag{5}$$

In these narrow avoided crossings, the peaks of the corresponding radial couplings can be fitted to (Landau-Zerer-type) Lorentzian functions:

$$\left\langle \phi_k \left| \frac{\partial}{\partial R} \right| \phi_{k+1} \right\rangle \simeq \frac{\delta/2}{\delta^2 + (R - R_0)^2} \tag{6}$$

with two parameters δ and R_0. Expressions (4)-(6) define the transformation angle α, and, in practice, some avoided crossings are so narrow that the corresponding couplings can be approximated by a delta function. To illustrate the accuracy of this transformation, we have over-imposed the energy of the "diabatic" entrance channel to the adiabatic ones in fig. 1a. Using this diabatic basis, we have found that transitions from the entrance channel to the exit ones whose energies cross that of the entrance channel at $R > 5.0\mathrm{a}_0$, are very small; so that these states have no been included the basis. The "diabatic" entrance channel is de-populated by transitions in the avoided crossing region at $R \simeq 3\mathrm{a}_0$, which lead to DSEC, and we have included in the dynamical calculation three DSEC channels, whose energies (see figure 1b), have been obtained by diabatizing a few narrow avoided crossings at short R.

The energies of the lowest two-electron capture channels are shown in fig. 1b. Direct transitions from the entrance channel to these states are not significant at $R \geq 3.0\mathrm{a}_0$, and TEC takes place mainly through a two- step process via $\mathrm{He}^+(1\mathrm{s})\ \mathrm{H}_2^{+*}$ (electronically excited) states. The energies of the $\mathrm{He}^+(2\mathrm{l})\ +\ \mathrm{H}_2^+(1\sigma_g)$ manifold do not cross that of the entrance channel, and the most important coupling appears between the first state of this manifold

and the entrance channel at R $\simeq$ 5 a_0, suggesting that single electron capture to that manifold is basically independent of DSEC, in which $He^+(1s)$ is formed. Finally, our basis set includes 10 "diabatized" channels, whose energies are presented in figure 1b.

To illustrate the variation of the molecular energies with R, ρ and θ, we show in figs. 2 and 3 the potential energy surfaces of the entrance channel and the state dissociating into $He^+(1s) + H_2^+(2\sigma_g)$ when $R \to \infty$. In these figures, the energy surface of the entrance channel has been obtained by traversing diabatically the sharp avoided crossing for each value of ρ and θ, as explained before for ρ=1.4a_0 and θ=45^0 (see figs. 1a,b). At $R >$3a_0 the upper energy surface decreases as $-2/R$ because this term has been subtracted from the calculated energy, which is almost constant; this surface practically does not change with ρ. At $R \simeq$2.5a_0, the upper surface shows a ridge that is a consequence of the avoided crossing with the next surface, which is not shown in this figure, but is noticeable in figure 1. The low-lying surface decreases as $-1/R$ for $R \gtrsim$2.5a_0, and it rapidly decreases when ρ increases, for all values of R, showing that the dissociative character of the molecular orbital $2\sigma_g$ is not appreciably changed by the interaction with He^+. Accordingly, the energy gap between the two surfaces in the avoided crossing along the line $R \simeq 3.0a_0$ becomes wider as ρ increases. A second avoided crossing at $R \simeq 1.5$ a_0, is hardly visible in figure 2 because of the fast increase of both surfaces at low R, but is clearly shown in figure 3(a), where we have plotted the difference between these two potential energy surfaces. Since the variation of the surfaces with the angle θ is less significant than on ρ, a common plot of these surfaces as functions of R and θ, similar to figure 2, is unclear and we only illustrate the corresponding difference in figure 3(b). In general, the anisotropy of the energy surfaces is only appreciable for $R \lesssim 2a_0$.

In figures 4 and 5 we illustrate the shape of the corresponding radial:

$$M_{ik} = \left\langle \phi_i \left| \left. \frac{\partial}{\partial R} \right|_{\rho,\theta} \right| \phi_k \right\rangle \tag{7}$$

and rotational couplings:

$$R_{ik} = \frac{1}{R} \left\langle \phi_i \left| \left. \frac{\partial}{\partial \theta} \right|_{\rho,R} \right| \phi_k \right\rangle , \tag{8}$$

where ϕ_i, ϕ_k are the molecular states whose energies have been plotted in figs. 2 and 3. The main structures of these couplings in figure 5 are due to the ridges in the avoided crossing

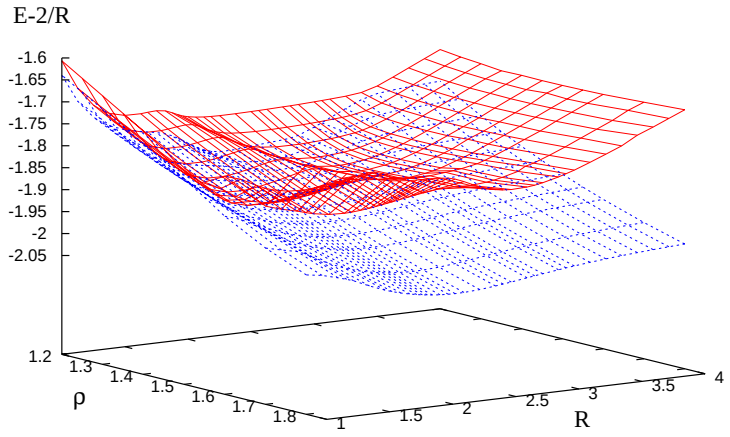

FIG. 2: Potential energy surfaces of the entrance channel and the state dissociating into $He^+(1s)$ + $H_2^+(2\sigma_g)$ when $R \to \infty$, as functions of ρ and R, for θ=45^0.

regions of 3a. In particular, the transitions in the avoided crossing region at $R \simeq 3a_0$ are a basic mechanism of the DSEC reaction. Regarding these transitions, both the decrease of the couplings and the increase of the energy gap lead to smaller non-adiabatic transitions when ρ increases. The opposite situation is found for the inner avoided crossing (at $R \simeq$ 1.5 a_0), where the avoided crossing becomes narrower as ρ increases, but since this avoided crossing is only traversed at very small impact parameters, the corresponding transitions are irrelevant to total charge transfer cross section calculations. As for the potential surfaces, the dependence of dynamical couplings on θ (fig. 5) is less marked than that on ρ.

III. DYNAMICAL METHOD.

A. *ab initio* treatment.

We employ the impact parameter method, in which the position vector $\mathbf{R}$ of the incident ion with respect to the target molecule follows straight-line trajectories with constant velocity $\boldsymbol{v}$ and impact parameter $\boldsymbol{b}$ in the collision (XZ) plane: $\mathbf{R} = \boldsymbol{b} + \boldsymbol{v}t$. The remaining degrees of freedom are treated quantum mechanically, by means of the wavefunction $\Psi(\boldsymbol{r}, \boldsymbol{\rho}, t)$, where

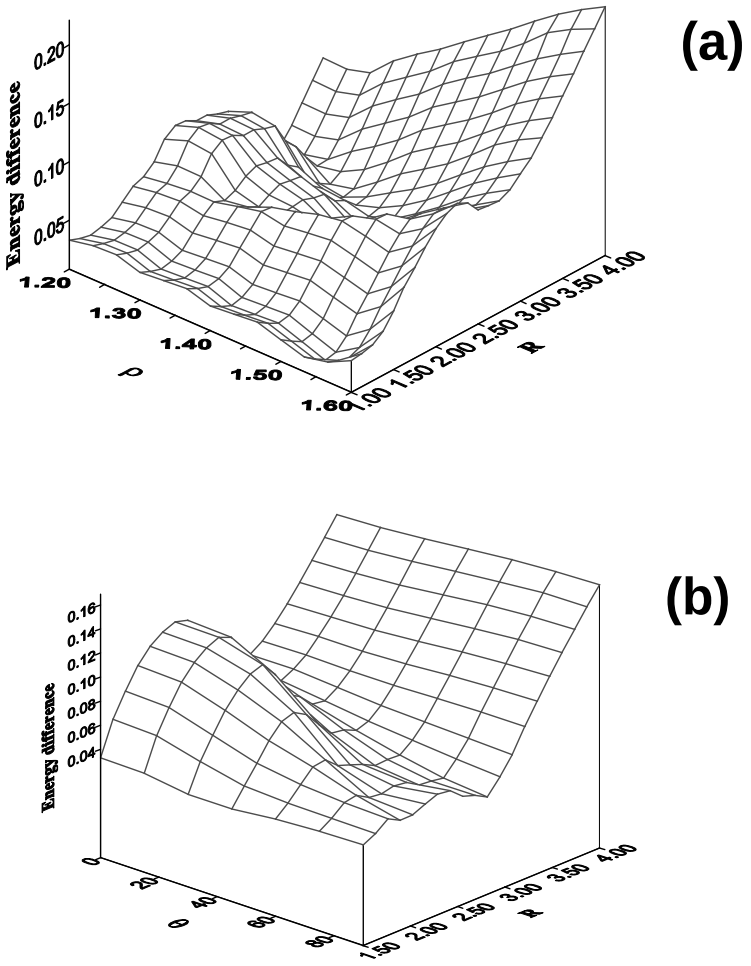

FIG. 3: (a) Difference between the energies of the states of fig. 2 as functions of ρ and R, for θ=45^0. (b) Same energy difference as function of θ and R for $\rho = 1.4$.

$\boldsymbol{r}$ denotes the set of electronic coordinates and Ψ is a solution of the equation:

$$\left(H_{\rm i} - {\rm i}\frac{\partial}{\partial t}\Big|_{\boldsymbol{r},\boldsymbol{\rho}} \right) \Psi(\boldsymbol{r},\boldsymbol{\rho},t) = 0 \tag{9}$$

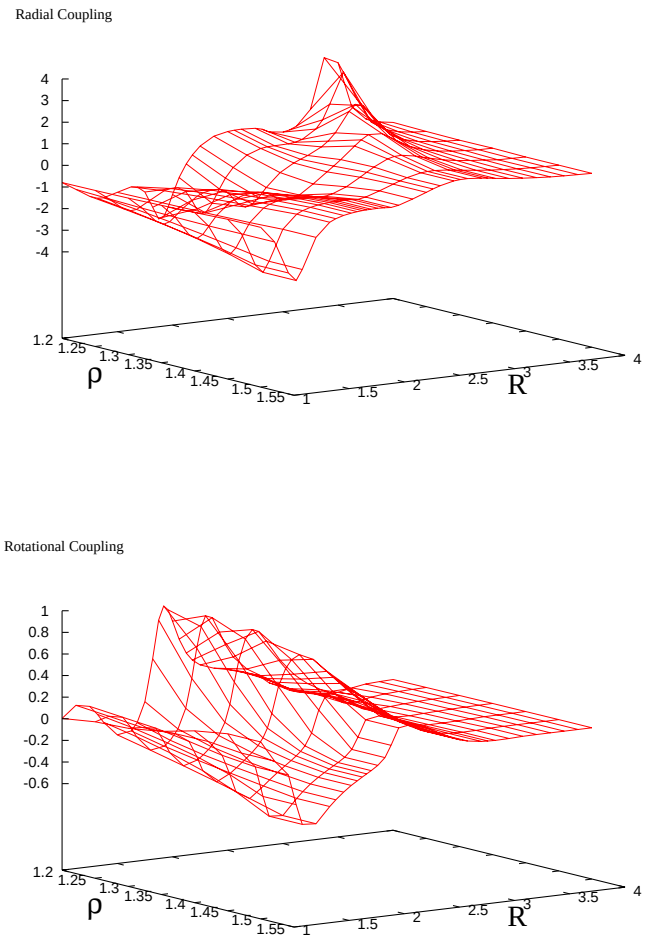

FIG. 4: Dynamical couplings between the entrance channel and the state dissociating into $He^+(1s)$ + $H_2^+(2\sigma_g)$ when $R \to \infty$, as functions of R and ρ, for θ=45^0.

with $\partial/\partial t = \boldsymbol{v} \cdot \nabla_R$ and

$$H_{\rm i} = -\frac{1}{2\mu}\frac{\partial^2}{\partial \rho^2} + H_{\rm elec} \tag{10}$$

The operator $H_{\rm elec}(\boldsymbol{r};\boldsymbol{\rho},\mathbf{R})$ is the Born-Oppenheimer electronic Hamiltonian, for fixed $\boldsymbol{\rho}$ and $\mathbf{R}$ values.

Within the FC approximation one expands Ψ in terms of the eigenfunctions of the electronic Hamiltonian, fulfilling $H_{\rm elec}\phi_j = \epsilon_j \phi_j$ in the form:

$$\Psi(\boldsymbol{r},\boldsymbol{\rho},t) = \rho^{-1} Y_{JM}(\hat{\rho})\chi_0(\rho)\exp({\rm i}U)\sum_j a_j(t;\boldsymbol{\rho_0})\ \phi_j(\boldsymbol{r},\boldsymbol{\rho_0},\mathbf{R})\ \exp\left[-{\rm i}\int_0^t \varepsilon_j {\rm d}t'\right] \tag{11}$$

where we assume that the initial ro-vibrational wavefunction $\chi_0(\rho)Y_{JM}(\hat{\rho})$ does not appre-

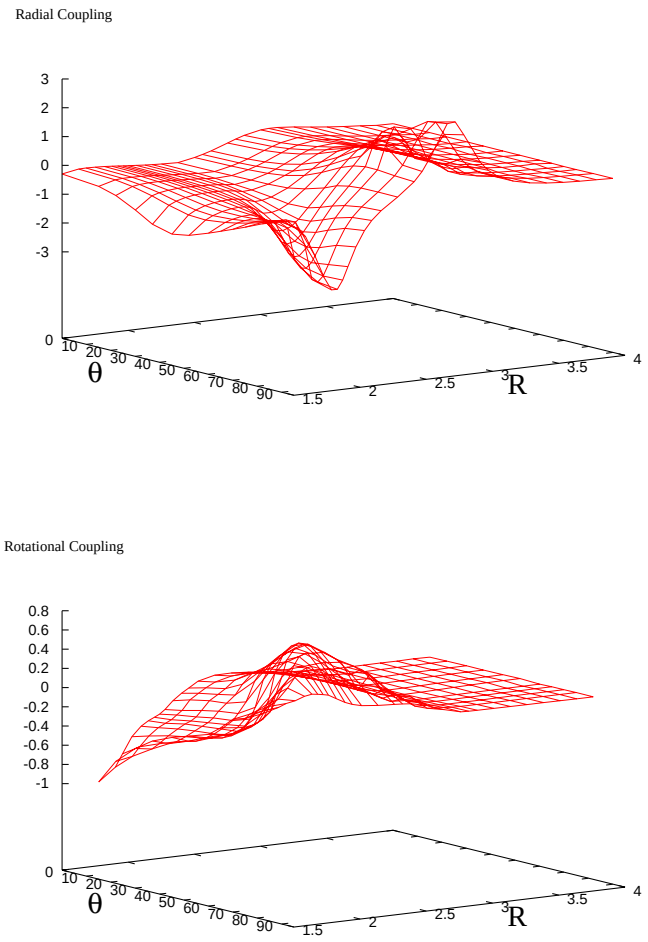

FIG. 5: Same couplings as in fig. 4 as functions of θ and R, for ρ=1.4a$_0$.

ciably change in the time interval in which the electronic transition takes place, and the the internuclear distance is fixed at the equilibrium H-H distance ρ_0= 1.4a$_0$ in the electronic wavefunctions. exp(i$U(\boldsymbol{r}_1, \boldsymbol{r}_2, t)$ is a common translation factor (CTF) [31]. In the *ab initio* treatment, we have employed the CTF of ref. [25]. The expansion coefficients $a_j(t; \boldsymbol{\rho_0})$ are obtained by substituting expansion (11) in eq. (9). For each nuclear trajectory one obtains:

$$\mathrm{i}\frac{\mathrm{d}a_j}{\mathrm{d}t} = \sum_k a_k \left\langle \phi_j \exp(\mathrm{i}U) \left| H_{\mathrm{elec}} - \mathrm{i}\frac{\partial}{\partial t} \right| \phi_k \exp(\mathrm{i}U) \right\rangle \exp\left[-\mathrm{i}\int_0^t (\varepsilon_k - \varepsilon_j)\mathrm{d}t'\right] \qquad (12)$$

where the dynamical couplings, which include the CTF corrections, are related to the radial and rotational couplings of eqs. (7) and (8) through the relationship (see [32]):

$$\left\langle \phi_j \exp(\mathrm{i}U) \left| H_{\mathrm{elec}} - \mathrm{i}\frac{\partial}{\partial t} \right| \phi_k \exp(\mathrm{i}U) \right\rangle = \frac{v^2 t}{R} M_{jk} - \frac{bv}{R} R_{jk} +$$

$$+\left\langle \phi_j \left| \sum_{i=1}^{2} \left[-\mathrm{i}\nabla_i U \cdot \nabla_i - \frac{\mathrm{i}}{2}\nabla_i^2 U + \frac{1}{2}(\nabla_i U)^2 \right] + \frac{\partial U}{\partial t} \right| \phi_k \right\rangle \tag{13}$$

The orientation-averaged transition probability to the vibronic final state $\phi_f \chi_{\nu'_f}$ is [2]:

$$P_{\nu' f}(\boldsymbol{b}, v) = (4\pi)^{-1} \int P_{\nu' f}(\boldsymbol{b}, v, \hat{\rho}) \boldsymbol{d}\hat{\rho} \tag{14}$$

where the orientation-dependent transition probability $P_{\nu' f}$ ($\boldsymbol{b}$, v, $\hat{\boldsymbol{\rho}}$) from the $\{\nu_i\}$ to the $\{\nu_f{}'\}$state is given by:

$$P_{\nu' f}(\boldsymbol{b}, v, \hat{\rho}) = |a_f(\infty; \boldsymbol{\rho_0})|^2 \left[\int \boldsymbol{d}\rho \chi_\nu(\rho) \chi_{\nu'}(\rho) \right]^2 \tag{15}$$

When the vibrational distribution is not required, the cross section for transition to a given electronic channel is:

$$\sigma_f(v) = (4\pi)^{-1} \int \mathrm{d}\boldsymbol{b} \int \mathrm{d}\hat{\rho} \sum_{\nu'} \boldsymbol{P}_{\nu' f}(\hat{\rho}, \boldsymbol{b}, \boldsymbol{v}) = (4\pi)^{-1} \int \mathrm{d}\boldsymbol{b} \int \mathrm{d}\hat{\rho}\, |a_f(\infty; \boldsymbol{\rho_0}) - \delta_{if}|^2 \tag{16}$$

The evaluation of the orientation averaged cross section of (16) requires to solve the system of differential equations (12) for several orientations of the vector $\boldsymbol{\rho}$ with respect to the nuclear velocity $\boldsymbol{v}$. Along the trajectory the angle θ between vectors $\boldsymbol{R}$ and $\boldsymbol{\rho}$ changes, which in practice requires the evaluation of the molecular wavefunctions ϕ_j in a grid of values of this angle. A simplification of this procedure has been studied in previous work [2, 33, 34], where we have shown that a good approximation to the orientation averaged cross sections is given by an isotropic approximation where the molecular wavefunctions of expansion (11) are assumed to be independent on θ, and one employs the molecular data calculated for an intermediate value (between 45 ° and 60 °). In this work we have used this isotropic approximation with $\theta = 45°$, where

$$\sigma_f(v) = 2\pi \int_0^\infty b P_f(b) \mathrm{d}b = \int_0^\infty b \left| a_f(\infty; \rho_0, \theta = 45^0) - \delta_{if} \right|^2 \mathrm{d}b \tag{17}$$

B. Independent particle model treatment.

As has been discussed in several publications on ion-atom collisions (see [35] and references therein), the usefulness of the close-coupling expansion (11), which does not include pseudostates, is limited at high energies by the competition of ionization processes. In general, the ionizing flux that cannot be correctly described by the basis overpopulates the

highest capture states, and calculated electron capture cross sections are overestimated by an amount similar to the ionization cross section. As mentioned in the introduction, at these energies, when ionization starts to be sizeable, we have applied the IPM method (see refs.[36, 37]). Here we summarize the main points of its application to He^{2+}-H_2 collisions. Our treatment starts by replacing the H_2^+ core by an effective one-centre potential $V_{\rm ef}(r_H)$, where $r_{\rm H}$ is the electron distance to the midpoint of the H-H internuclear axis. The resulting one-electron Hamiltonian has the form:

$$h = -\frac{1}{2}\nabla^2 - \frac{2}{r_{\rm He}} + V_{\rm ef}(r_{\rm H}) \tag{18}$$

where $r_{\rm He}$ is the electron distance to the He nucleus. In practice we have employed two effective potentials: a model potential of the form:

$$V_{\rm ef} = -\frac{1}{r_{\rm H}} - \frac{1}{r_{\rm H}}(1+\alpha r_{\rm H})\exp(-2\alpha r_{\rm H}) \tag{19}$$

and the Coulomb potential created by an effective charge $Z_{\rm eff}$=1.0995, where both parameters α= 3.93 and $Z_{\rm eff}$ were chosen so as to fit the H_2 ionization potential for a fixed internuclear distance of $1.4a_0$, consistent with the FC approximation. We have checked that both effective potentials lead to practically identical cross sections, and only one set of results will be presented in the next sections.

The one-electron impact parameter equation:

$$\left(h - \mathrm{i}\left.\frac{\partial}{\partial t}\right|_{\boldsymbol{r}}\right)\Phi(\boldsymbol{r},t) = 0 \tag{20}$$

is then solved with the appropriate initial condition, yielding one-electron probabilities: $p_{\rm el}$, $p_{\rm ex}$, $p_{\rm c}$ and $p_{\rm i}$ for elastic, excitation, capture and ionization probabilities, respectively; these are then used to evaluate the transition probabilities for the physical two-electron problem, by means of the equivalent electron interpretation [38–40]. In particular, if one electron remains in the initial H_2^+ molecular orbital $1\sigma_g$, the H_2^+ ion does not dissociate, leading to:

$$P_{\rm NDSEC} = 2p_{\rm c}p_{\rm el};\ P_{\rm NDI} = 2p_{\rm i}p_{\rm el} \tag{21}$$

for the probabilities of non-dissociative electron capture, $P_{\rm NDSEC}$ and non-dissociative ionization, P_{NDI}. Similarly, for reactions (2) and (3), we have in principle:

$$P_{\rm TEC} = p_{\rm c}^2\ ;P_{\rm DSEC} = 2p_{\rm c}p_{\rm dis}\,, \tag{22}$$

where $p_{\rm dis}$ is the probability for excitation to H_2^+ dissociative molecular orbitals. However, it is well known (see [41] and references therein, [37, 42–44]) that the IPM approach is not appropriate to evaluate cross sections for two-electron processes like TEC and DSEC, and we expect that expressions (22) will lead to inaccurate results.

The total cross sections for a given process are then given by:

$$\sigma_k(v) = 2\pi \int_0^\infty bP_k(b,v)\mathrm{d}b \tag{23}$$

where P_k is any of the probabilities obtained from eqs. (21) and (22).

In the present calculation, the wavefunction Φ is expanded in a set of 14 molecular orbital (OEDM) of the HeH^{2+} system [13] and 90 Gaussian pseudostates as defined in ref. [14], and including the CTF of Harel and Jouin [45]. The inclusion of pseudostates in this treatment improves the description at high v, where ionization starts to compete with electron capture.

IV. DYNAMICAL CALCULATIONS

Our results for total electron capture (the sum of DSEC and NDSEC) cross sections are plotted in figure 6 compared to the experimental data [5, 18, 19, 21]. In this figure we have included the experimental data of Shah *et al.* [5] for total ionization (the sum of dissociative, non-dissociative and transfer ionization cross sections), which indicate that the high E limit of our *ab initio* calculation, (not including pseudostates) in the basis set, is E >10 keV/amu. For lower energies, our results are higher than the experimental data but we find a similar energy dependence, with the exception of the cross sections of Nutt *et al.* [18] that decrease more rapidly at low energies. The IPM results show general good agreement with the experimental data in the energy range shown in figure 6.

In our 10-state ab initio basis set of fig. 1, the cross sections for NDSEC are identical to those for reaction:

$$He^{2+} + H_2 \rightarrow He^+(2s, 2p) + H_2^+(1\sigma_g) \tag{24}$$

and those for DSEC are for reactions:

$$He^{2+} + H_2 \rightarrow He^+(1s) + H_2^+(2\sigma_g, 2\sigma_u, 3\sigma_g) \tag{25}$$

Our results in this basis (see figure 7a) agree with the conclusions of the experimental works of Hodgkinson *et al.* [4] and Shah *et al.* [5], which pointed out that DSEC is the dominant

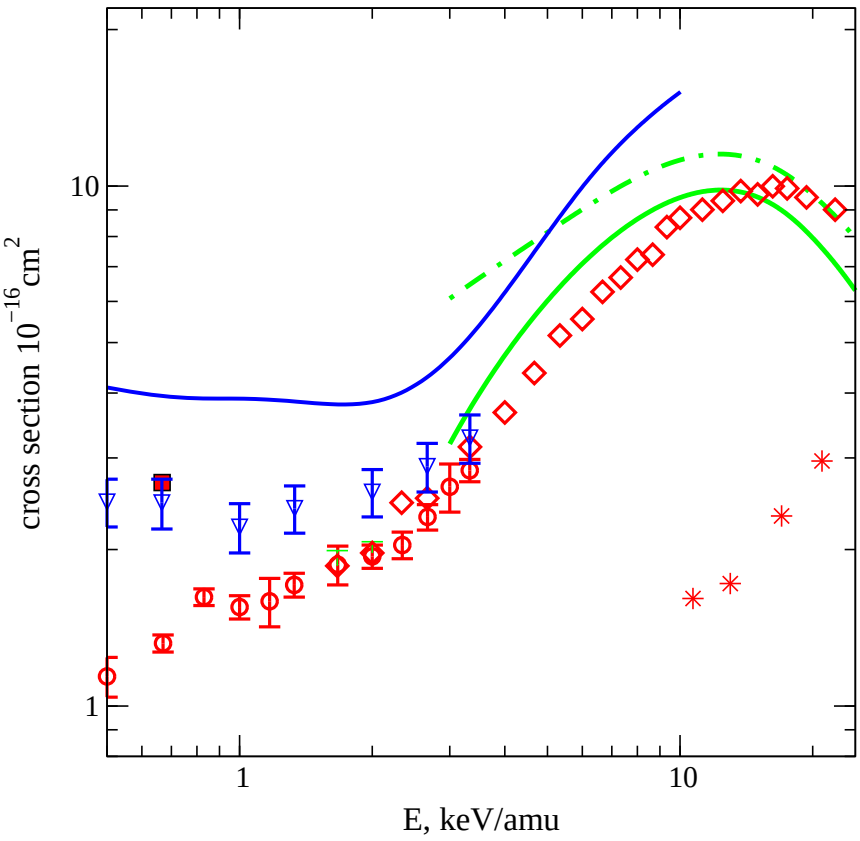

FIG. 6: Total cross sections for single electron capture: Full line, present results (black line, *ab initio* calculation, gray line, IPM calculation); ◇, [17] ; ◯, [18]; ▽,[19]; ■, [21]. ⋆, cross section of [5] for ionization. The dashed-dotted line has been obtained by adding to the IPM cross section the *ab initio* one for DSEC.

process at low v, and NDSEC at $E \gtrsim$10keV/amu, and do not agree with those of ref. [7], which suggested that NDSEC was the dominant process at $E \lesssim$ 1keV/amu.

We have included in figure 7 the cross section values for single electron capture of [19] and [21] previously shown in figure 6, and which must be identical to those for DSEC at $E <$2keV/amu, since NDSEC cross sections are very small at low v. We have also plotted in figure 7 the total cross sections of Graham *et al.* [46] for protons production; this includes DSEC, TEC, transfer ionization and dissociative ionization. In this respect, as pointed out in ref. [22], the sum of cross sections of [5] for DSEC, transfer ionization and dissociative ionization (also shown in figure 7), and those of ref. [17] for TEC, reasonably agree with the values of ref. [46] at $E \gtrsim$10keV/amu. Ionizing processes are not relevant at $E \lesssim$5keV/amu, and TEC cross sections (see figure 10) are also very small, so that the results of ref. [46]

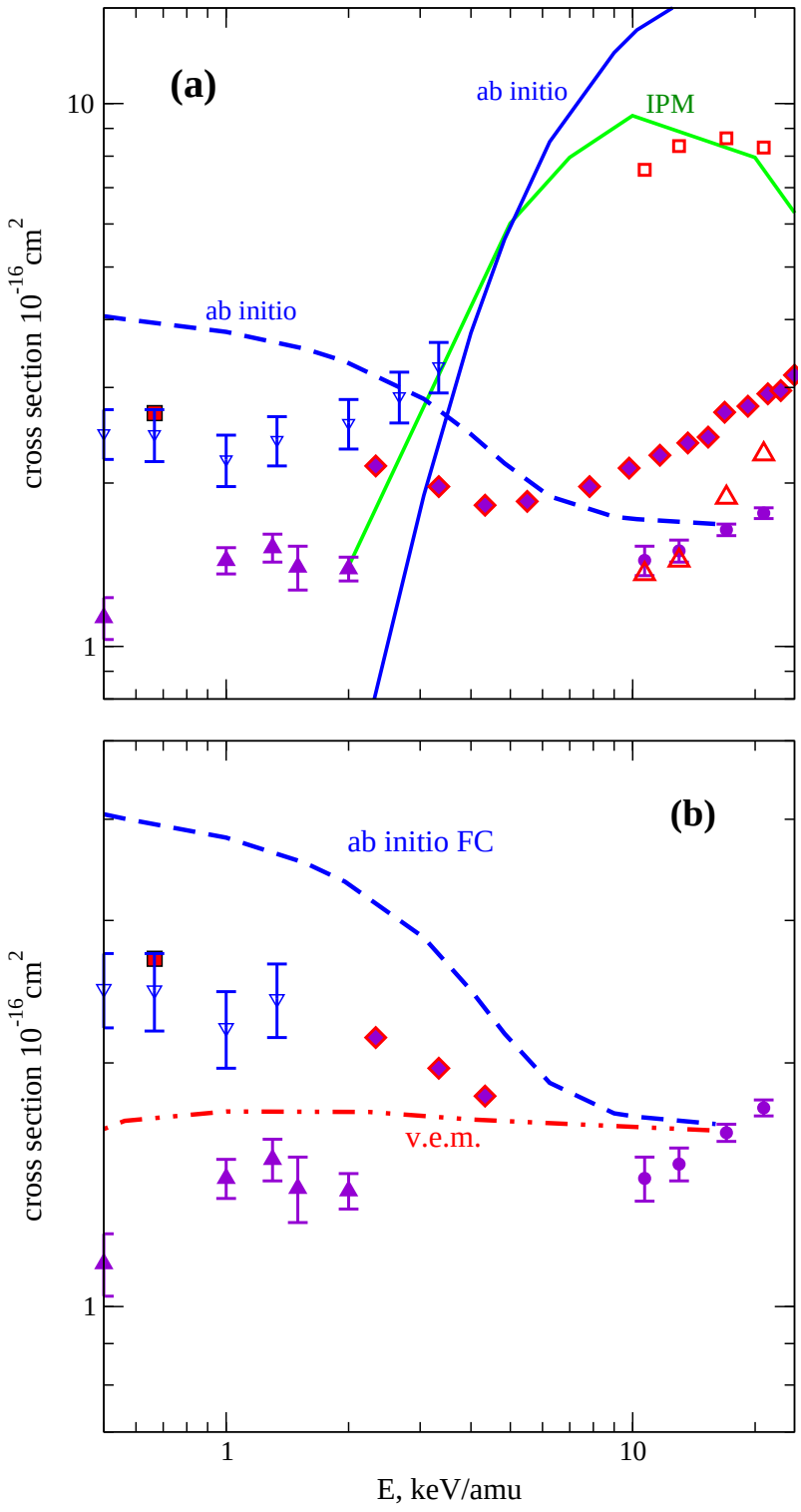

FIG. 7: (a)Total cross sections for NDSEC: Full lines, present results; □, [5] Total cross sections for DSEC: Dashed line, present results; ▲, [4], •, [5]. ⧫, cross section for production of protons of [46]. Experimental data for total cross section: ▽, [19]; ■, [21]. △, sum of cross section for dissociative ionization and transfer ionization of [5] (b)Total cross sections for DSEC: - ·· -, two-state vibrational excitation model. Other symbols as in (a). Note the slightly different ordinate scales.

can be taken as a measure of DSEC cross sections at these impact energies.

To further study the comparison of different results for DSEC, we have plotted in figure 7b our results together with those experimental values that are either direct measurements of the DSEC cross section [4, 5] or, as explained above, an indirect measurement of this cross section in a given energy range [19, 21, 46]. It can be noted that experimental and calculated values show similar energy dependences, although the latter are larger, in particular at low v. This comparison seems to point out to an underestimate of the DSEC cross section in the work of ref. [4], probably as a consequence of a corresponding difficulty in the data of ref. [18] (see figure 6) that were used to normalize it.

A possible source of error in our calculation is the neglect of vibrational effects. In this respect, to gauge the effect of the FC approximation on our results for DSEC, we have carried out a model calculation including two electronic states: the entrance channel and the most important exit channel (the state dissociating into $He^+(1s)+ H_2^+(2\sigma_g)$), whose energies and dynamical couplings are plotted in figs. 2- 5. We have checked that, for $E < 3$keV/amu, this two-state basis set yields a single capture cross section at the FC level with the same shape and about 25% smaller than that from the 10-state basis set. Within this reduced basis we have approximately included vibrational effects by employing the model (v.e.m.) of appendix A, and whose results are included in figure 7b. In this model the initial vibrational function χ_0 of eq. (11) is replaced by a superposition of vibrational states of the H_2 molecule, that describes vibrational excitation during the collision. The observed decrease of the cross section with respect to the FC one indicates that the discrepancy of our results with that of [19] for $E \lesssim 1$keV/amu is due to the use of the FC approach.

We finally mention that the IPM calculation lead to negligible DSEC cross sections (not shown in figure 7), which is an unphysical result due to the limitations of the IPM approximation. In particular, as mentioned in section III B, DSEC involves, besides electron exchange, the excitation of the second electron to a dissociative molecular orbital, so that DSEC is a two-electron process that is not accurately described by this method. The IPM cross sections for NDSEC of figure 7 are indistinguishable from the total capture cross section of figure 6 and agree with the corresponding experimental values of Shah *et al.* [5] at $E >10$keV/amu. An estimate of the IPM result for total capture single capture cross section at high v can be obtained (see [8]) by adding to the IPM one for NDSEC, the *ab initio* DSEC cross section, which is also shown in figure 6.

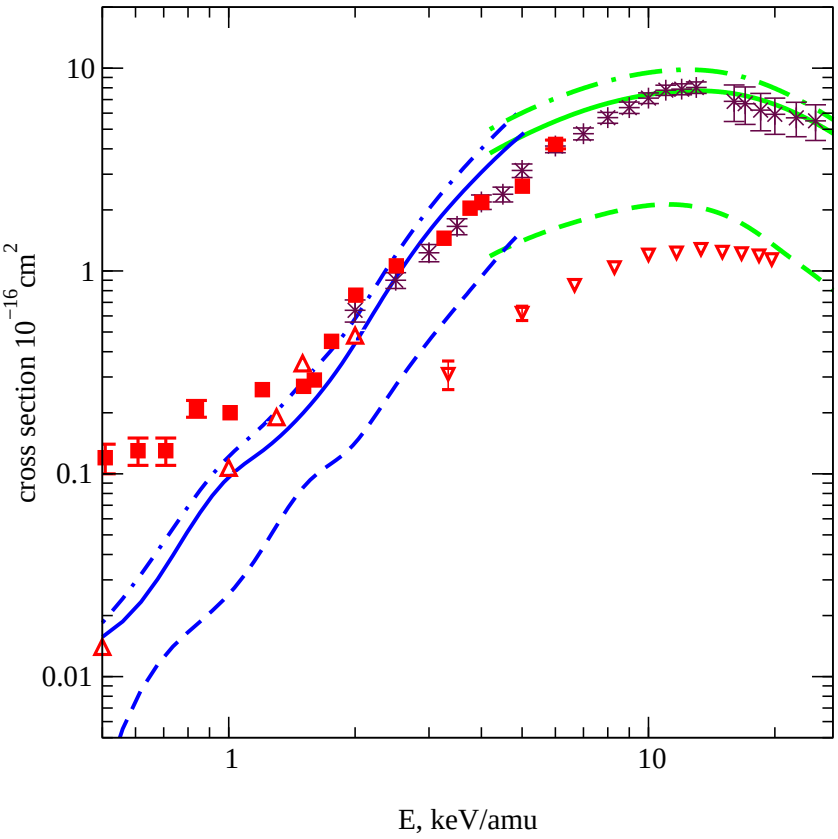

FIG. 8: Cross sections for NDSEC into $He^+(2l) + H_2^+(1\sigma_g)$: Dashed-dotted line, present results; △, experimental data of [4]. Cross sections for NDSEC into $He^+(2s) + H_2^+(1\sigma_g)$: Dashed line, present results; ▽, experimental data of [16]. Cross sections for NDSEC into $He^+(2p) + H_2^+(1\sigma_g)$: Full line, present results; ■, [24], ⋆, [22]. •, experimental data of [5] for NDSEC cross section. Black lines are *ab initio* results; gray lines, IPM results

In figure 8 we present our calculated cross sections for the reactions (24) along with experimental data [4, 16, 24]. As for total electron capture, the IPM approach is appropriate at high E and the *ab initio* treatment at low E, and accordingly we have plotted in this figure our more accurate values in each energy range (see [8]). The only remarkable discrepancy in figure 8 is the large difference between the measurements of refs. [24] and [4] at $E \lesssim$1keV/amu., which, as already noted by Juhász *et al.* [24], is not solved even assuming a factor of two of error in the normalization of the data of ref. [4], as might be suggested by the comparison of figure 6. Although the accuracy of our results at low v is limited by the use of the FC approximation, they agree with those of Hodgkinson *et al.* [4].

To study the mechanism of reactions (24), we have checked that the cross section cal-

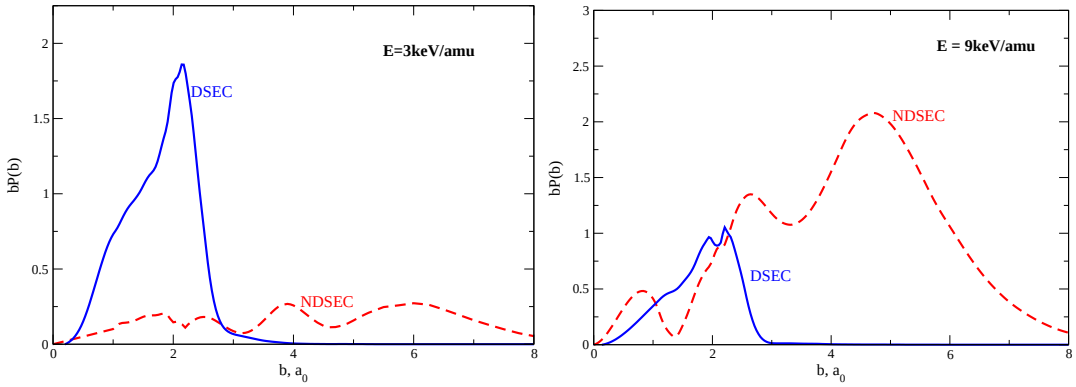

FIG. 9: $bP(b)$ as function of b for two impact energies Full line, probability of DSEC; dashed line, probability of NDSEC.

culated with a 4-state basis, including the entrance channel and those dissociating into $He^+(2l)+H^{2+}(1\sigma_g)$, are practically indistinguishable from those presented here from the 10-state calculation; this confirms the indication from the energy correlation diagram of figure 1b that reactions (24) are independent of the other single and double electron capture ones, and takes place through transitions at $R \simeq 5.0$ a.u. from the entrance channel to the lowest state of the multiplet that correlates to $He^+(2l)+ H_2^+(1\sigma_g)$ when $R \to \infty$. An illustration of the mechanisms is shown in figure 9, where we compare the probabilities of DSEC and NDSEC at two impact energies to show that these two processes take place in different impact parameter ranges. Since transition leading to reactions (24) occur at relatively large internuclear distances, where the distortion of the H-H interaction potential by the interaction with the He^{2+} ion is relatively small, we expect that the effect of vibrational excitation to be less significant than for reaction (2) and consequently we expect more accurate results for this subdominant reaction than for the dominant (DSEC) one. Nevertheless, a detailed vibronic close-coupling calculation is required in order to analyze the possibility of an alternative quasiresonant vibronic mechanism, as found in H^+-H_2 collisions [3], that might explain the increase at low v of the cross section in the experiment of [24].

We show in figure 10 the calculated total cross section, for reaction (3), calculated using the *ab initio* treatment. Our total cross section shows a two-peak structure, similar to that obtained by joining the cross sections from the experiments of Kusakabe *et al.* [19] and Shah and Gilbody [17]. Although we do not obtain the small experimental values at 2-3 keV/amu, good agreement is found near the maxima. The shape of the TEC cross section

is a consequence of the two-step mechanism of this reaction. In particular, at low v, TEC channels are populated at small R through transitions in the neighborhood of the avoided crossings with DSEC channels, and the decrease of the TEC cross section at $E \simeq 1$keV/amu is a consequence of the decrease of the DSEC cross section (see fig 7). The increase of the TEC cross section for $E \gtrsim 2$keV/amu is due to two new mechanisms: The first one involves the transition from the state correlated to $He^+(1s)+ H_2^+(3\sigma_g)$ to the state leading to $He(1s2s)+H_2^{2+}$ at a broad avoided crossing at $R \simeq 6.0a_0$. In the second mechanism the channels dissociating into $He^+(2l)+ H_2^+$ are populated in the first step. In this respect, it can be noted that the TEC cross section increases in the energy region where the NDSEC one also increases. To illustrate this mechanism, we have checked that canceling the dynamical couplings between NDSEC and TEC channels yields a significant reduction of the cross section for $E \gtrsim 1$keV/amu (see figure 10), while it is unchanged at low v. In contrast with the known mechanisms of TEC in collisions of multicharged ions with He [47–51], we do not find in this system the simultaneous exchange of both electrons. The relatively good agreement of calculated and experimental TEC cross sections at low v can be explained, as for reaction (24), as a consequence of the mechanism of this process, where TEC channels are populated in the first part of the collision where vibrational excitation is still not very important.

V. CONCLUSIONS.

We have applied the FC approximation with *ab initio* and IPM approaches to evaluate single and double capture cross sections in the energy range 0.5-2.5keV/amu. In this energy range, some of the computational characteristics of this system, such as the presence of infinitely excited states, the competition between single and double capture, and the need to include pseudostates at high v are common to ion-H_2 and ion-atom (eg. He) collisions, but are non-standard applications of Quantum Chemistry techniques in the former case. In addition, the vibrational structure and the fact that the main exit channels are dissociative, implies that in principle one expects less accurate results of the present calculation than for two-electron ion-atom systems.

In this work, we have presented a detailed account of the calculation of potential energy surfaces and dynamical couplings to illustrate the way we apply a CI method to this kind of

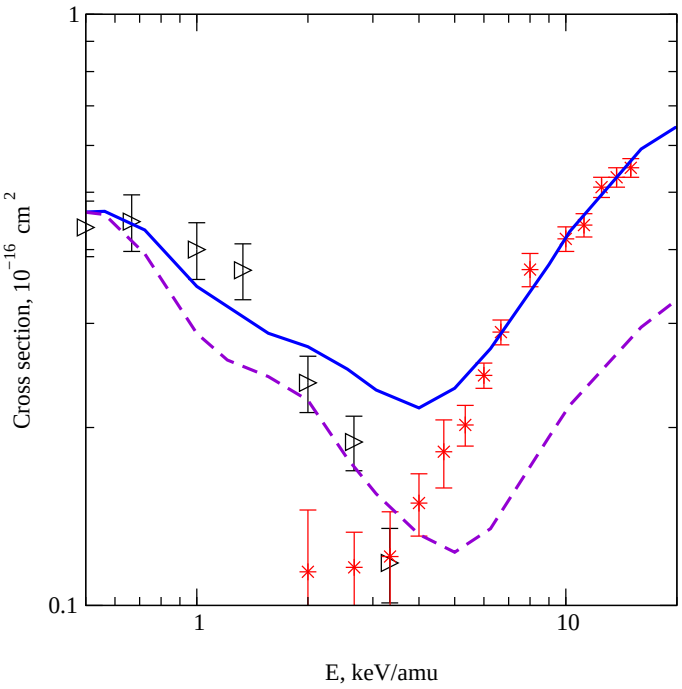

FIG. 10: (a)Cross sections for two-electron capture: — , present results; - - - , Present results removing the couplings between states dissociating into $He^+(2l)+H^{2+}(1\sigma_g)$and TEC states. Experimental data: ▷, [19]; ⋆, [17].

problems. From the dynamical point of view, our calculation employs the FC approximation, and this limits the energy range to E >500 eV/amu, since we have shown some indications of non FC vibrational effects at higher energies, specially for DSEC using the model explained in the appendix. In the energy range of the present work, DSEC and NDSEC take place through independent mechanisms, which allows to evaluate the corresponding cross sections separately, and as a consequence, to employ the IPM approach to treat NDSEC, where it is most accurate, using a large OEDM basis augmented with pseudostates.

With respect to the comparison with experimental data, our results agree with the general trend of one- and two-electron capture cross sections and also show reasonable agreement with partial cross sections. Nevertheless , further experimental and theoretical work is required to solve some discrepancies. In particular, our results for total electron capture from both (*ab initio* and IPM) approaches are larger than the experimental ones at $E \simeq$ 4keV/amu, where our experience with other ion-H_2 collisions suggests that the FC approximation should be appropriate, and where we find better agreement by comparing DSEC and NDSEC components. At lower energies our cross sections show better agreement with the

results of ref. [19] than with those of ref. [18]. Finally, our calculation does not reproduce the results of [24] for formation of $He^+(2p)$, but further work is required to solve the striking discrepancy between the experiments of [4] and [24]; in particular, a vibronic close coupling treatment is needed to accurately describe vibrational effects.

APPENDIX A: VIBRATIONAL EXCITATION MODEL.

We consider an expansion of the form:

$$\begin{aligned}\Psi\ (\boldsymbol{r},\boldsymbol{\rho},t) &= \rho^{-1}Y_{JM}(\hat{\rho})\xi(\rho,t)\exp(\mathrm{i}U)\times \\ \times\ &\left[a_i(t)\ \phi_i^d\ \exp\left(-\mathrm{i}\int_0^t \varepsilon_i \mathrm{d}t'\right) + a_f(t)\ \phi_f^d\ \exp\left(-\mathrm{i}\int_0^t \varepsilon_f \mathrm{d}t'\right)\right] \end{aligned} \tag{A1}$$

where $\phi_{i,f}^d$ are two diabatic states which fulfill

$$\begin{aligned}\left\langle \phi_i^d \right| \left.\frac{\partial}{\partial R}\right|_\rho \left|\phi_f^d\right\rangle = 0 \\ \left\langle \phi_i^d \right| \left.\frac{\partial}{\partial \rho}\right|_{\boldsymbol{R}} \left|\phi_f^d\right\rangle = 0 \end{aligned} \tag{A2}$$

In eq. (A1) we have assumed, as an extension of the FC approximation of eq. (11), a common vibrational component $\xi(\rho,t)$ for both electronic states, whose time dependence allows us to describe the effect of the vibrational excitation that arises from the change of the molecular potential, due to the ion-molecule interaction. We express ξ as a linear combination of the H_2 vibrational wavefunctions $\chi_k(\rho)$:

$$\xi(\rho,t) = \sum_k c_k(t)\chi_k(\rho)\exp(-\mathrm{i}\epsilon_k t) \tag{A3}$$

with energies ϵ_k:

$$\left[-\frac{1}{2\mu}\frac{\partial^2}{\partial\rho^2} + V_0(\rho)\right]\chi_k(\rho) = \epsilon_k\chi_k(\rho)\ , \tag{A4}$$

and $V_0(\rho)$ is the energy of the H_2 ground electronic state. When the He^{2+} ion approaches, the potential $V_0(\rho)$ is changed by $V(\rho,t)$ which includes the ion-molecule interaction; this interaction induces transitions to the excited vibrational states, and, neglecting non-adiabatic electronic transitions, the vibrational wavefunction is solution of the time-dependent equation:

$$\left[-\frac{1}{2\mu}\frac{\partial^2}{\partial\rho^2} + V(\rho,t) - \mathrm{i}\frac{\partial}{\partial t}\right]\xi(\rho,t) = 0 \tag{A5}$$

Substitution of (A3) in (A5) leads to a system of differential equations for the coefficients c_k of the form:

$$\mathrm{i}\dot{c}_k = \sum_l c_l \langle \chi_k \mid (V - V_0) \mid \chi_l \rangle \exp[-\mathrm{i}(\epsilon_l - \epsilon_k)t] \tag{A6}$$

Assuming that the molecule is initially in the ground vibrational state χ_0, the system (A6) is solved with the initial condition $c_k(-\infty) = \delta_{k0}$. Substituting at each t the wavefunction (A1) in the semiclassical equation (9) yields a system of differential equations for the coefficients $a_k(t)$ whose integration leads to the electron capture cross sections, plotted in fig. 7b.

ACKNOWLEDGMENTS

This work has been partially supported by DGICYT projects BFM2000-0025 and FTN2000-0911.

---

[1] D. Elizaga, L. F. Errea, J. Gorfinkiel, C. Illescas, A. Macías, L. Méndez, I. Rabadán, A. Riera, A. Rojas, and P. Sanz, Atomic and Plasma-Material Interaction Data for Fusion **10**, 71 (2002).

[2] L. F. Errea, J. D. Gorfinkiel, A. Macías, L. Méndez, and A. Riera, J. Phys. B: At. Mol. Opt. Phys. **30**, 3855 (1997).

[3] L. F. Errea, A. Macías, L. Méndez, I. Rabadán, and A. Riera, Phys. Rev. A **65**, 010701(R) (2001).

[4] J. M. Hodgkinson, T. McLaughlin, R. W. McCullough, J. Geddes, and H. B. Gilbody, J. Phys. B: At. Mol. Opt. Phys. **28**, L393 (1995).

[5] M. B. Shah, P. McCallion, and H. B. Gilbody, J. Phys. B: At. Mol. Opt. Phys. **24**, 3983 (1989).

[6] B. C. Saha, N. F. Lane, and M. Kimura, Phys. Rev. A **44**, R1 (1991).

[7] N. Shikamura, M. Kimura, and N. F. Lane, Phys. Rev. A **47**, 709 (1993).

[8] L. F. Errea, A. Macias, L. Méndez, B. Pons, and A. Riera, J. Phys. B: At. Mol. Opt. Phys. p. in press (2003).

[9] L. F. Errea, J. D. Gorfinkiel, E. S. Kryachko, A. Macías, L. Méndez, and A. Riera, J. Chem. Phys. **106**, 172 (1997).

[10] L. F. Errea, J. D. Gorfinkiel, A. Macías, L. Méndez, and A. Riera, J. Phys. B: At. Mol. Opt. Phys. **32**, 1705 (1999).

[11] A. Macías and A. Riera, Phys. Rep. **81**, 299 (1982).

[12] A. L. Godunov, J. H. McGuire, P. B. Ivanov, V. A. Shipakov, H. Merabet, R. Bruch, J. Hanni, and K. K. Shakov, J. Phys. B: At. Mol. Opt. Phys. **34**, 5055 (2001).

[13] J. D. Power, Phil. Soc. Trans. R. Soc **274**, 663 (1973).

[14] L. F. Errea, C. Harel, H. Jouin, L. Méndez, B. Pons, and A. Riera, J. Phys. B: At. Mol. Opt. Phys. **31**, 3527 (1998).

[15] L. F. Errea, A. Macías, L. Méndez, and A. Riera, Phys. Rev. A **64**, 032714 (2001).

[16] M. B. Shah and H. B. Gilbody, J. Phys. B: At. Mol. Phys. **9**, 1937 (1976).

[17] M. B. Shah and H. B. Gilbody, J. Phys. B: At. Mol. Phys. **11**, 121 (1978).

[18] W. L. Nutt, R. W. McCullough, K. Brady, M. B. Shah, and H. B. Gilbody, J. Phys. B: At. Mol. Phys. **11**, 1457 (1978).

[19] T. Kusakabe, H. Yoneda, Y. Mizumoto, and K. Katsurayama, J. Phys. Soc. Jpn. **59**, 1218 (1990).

[20] K. Sato, K. Takiyama, T. Oda, U. Furukane, R. Akiyama, M. Mimura, M. Otsuka, and H. Tawara, J. Phys. B: At. Mol. Opt. Phys. **27**, L651 (1994).

[21] K. Okuno, K. Soejima, and Y. Kaneko, J. Phys. B: At. Mol. Opt. Phys. **25**, L105 (1992).

[22] R. Hoekstra, H. O. Folkers, J. P. M. Beijers, R. Morgenstern, and F. J. de Heer, J. Phys. B: At. Mol. Opt. Phys. **27**, 2021 (1994).

[23] G. Lubinski, Z. Juhász, R. Morgenstern, and R. Hoekstra, Phys. Rev. Lett. **86**, 616 (2001).

[24] Z. Juhász, G. Lubinski, R. Morgenstern, and R. Hoekstra, Atomic and Plasma-Material Interaction Data for Fusion **10**, 25 (2002).

[25] L. F. Errea, L. Méndez, and A. Riera, J. Phys. B: At. Mol. Opt. Phys. **15**, 101 (1982).

[26] J. F. Castillo, L. F. Errea, A. Macías, L. Méndez, and A. Riera, J. Chem. Phys. **103**, 2113 (1995).

[27] E. Davidson, in *MOTECC, Modern Techniques in Computational Chemistry*, edited by E. Clementi (ESCOM Publishers B. V., Leiden, 1990).

[28] L. Wolniewicz and K. Dreizler, J. Chem. Phys. **88**, 3861 (1988).

[29] C. E. Moore, *Atomic Energy Levels Nat. Stand. Ref. Data Series vol. 1* ((US National Bureau of Standards), 1971).

[30] F. T. Smith, Phys. Rev. **179**, 111 (1969).

[31] S. B. Schneiderman and A. Russek, Phys. Rev. **181**, 311 (1969).

[32] L. F. Errea, C. Harel, H. Jouin, L. Méndez, B. Pons, and A. Riera, J. Phys. B: At. Mol. Opt. Phys. **27**, 3603 (1994).

[33] L. F. Errea, A. Macías, L. Méndez, and A. Riera, J. Phys. B: At. Mol. Opt. Phys. **32**, 4065 (1999).

[34] L. F. Errea, A. Macías, L. Méndez, I. Rabadán, and A. Riera, Int. J. Mol. Sci. **3**, 142 (2002).

[35] L. F. Errea, C. Harel, H. Jouin, L. Méndez, B. Pons, A. Riera, and I. Sevila, Phys. Rev. A **65**, 022711 (2002).

[36] D. Elizaga, L. F. Errea, J. D. Gorfinkiel, L. Méndez, A. Macías, A. Riera, A. Rojas, O. J. Kroneisen, T. Kirchner, H. J. Lüdde, et al., J. Phys. B: At. Mol. Opt. Phys. **32**, 857 (1999).

[37] L. Errea, J. D. Gorfinkiel, C. Harel, H. Jouin, A. Macías, L. Méndez, B. Pons, and A. Riera, J. Phys. B: At. Mol. Opt. Phys. **33**, 3107 (2000).

[38] J. H. McGuire and L. Weaver, Phys. Rev. A **16**, 41 (1977).

[39] V. Sidorovich, J. Phys. B: At. Mol. Phys. **14**, 4805 (1981).

[40] H. J. Lüdde and R. M. Dreizler, J. Phys. B: At. Mol. Opt. Phys. **18**, 107 (1985).

[41] B. H. Bransden and M. H. C. McDowell, *Charge Exchange and the Theory of Ion-Atom Collisions* ((Oxford: Clarendon), 1992).

[42] R. Shingal and C. D. Lin, J. Phys. B: At. Mol. Opt. Phys. **24**, 251 (1991).

[43] M. McCartney, J. Phys. B: At. Mol. Opt. Phys. **30**, L155 (1997).

[44] C. Illescas and A. Riera, Phys. Rev. A **A60**, 4546 (1999).

[45] C. Harel and H. Jouin, J. Phys. B: At. Mol. Opt. Phys. **25**, 221 (1992).

[46] W. G. Graham, C. Latimer, R. Browning, and H. B. Gilbody, J. Phys. B: At. Mol. Phys. **7**, L405 (1974).

[47] N. Stolterfoht, C. C. Havener, R. A. Phaneuf, J. K. Swenson, S. M. Shafroth, and F. W. Meyer, Phys. Rev. Lett. **57**, 74 (1986).

[48] C. Harel and H. Jouin, Europhys. Lett. **11**, 2121 (1990).

[49] M. Barat, P. Roncin, L. Guillemot, M. N. Gaboriaud, and H. Laurent, J. Phys. B: At. Mol. Opt. Phys. **23**, 2811 (1990).

[50] L. F. Errea, B. Herrero, L. Méndez, and A. Riera, J. Phys. B: At. Mol. Opt. Phys. **28**, 693 (1995).

[51] X. Fléchard, C. Harel, H. Jouin, B. Pons, L. Adoui, F. Freémont, A. Cassimi, and D. Hennecart, J. Phys. B: At. Mol. Opt. Phys. **34**, 2759 (2001).